J. Fluid Mech. (1987), *vol.* 176, *pp.* 419–441
Printed in Great Britain

Convection in a vertical slot

By P. G. DANIELS

Department of Mathematics, The City University, Northampton Square, London EC1V 0HB, UK

(Received 24 October 1985 and in revised form 8 September 1986)

A boundary-layer approximation is used to describe the convective regime in a laterally heated vertical slot at large Prandtl numbers. The determination of the core flow requires the solution of the vertical boundary-layer equations in a rectangle, subject to appropriate boundary conditions on each of the four walls. Solutions based on a spectral decomposition in the vertical direction allow a comparison with experimental and numerical results, and an appraisal of an approximate solution frequently used as a basis for stability studies. Both the numerical results and an approximate stability argument lead to a simple criterion for the appearance of multiple rolls in the slot which appears to be in good agreement with experiments.

1. Introduction

The study of natural convection in a rectangular cavity whose lateral walls are held at different fixed temperatures is one of the classical problems of thermal convection (Nusselt 1909; Batchelor 1954; Elder 1965). For cavities of vertical aspect ratio $h \gg 1$, which are the main concern of the present paper, heat-transfer predictions are of relevance in the thermal insulation of walls and windows, and a more recent application is found in the cooling of nuclear reactors. The theoretical description of the flow in a vertical slot, based on the Boussinesq approximation, began with the analysis of the conductive regime by Batchelor (1954). The transfer of heat across the cavity by pure conduction leads to a horizontally stratified vertical core flow with a cubic velocity profile corresponding to upward motion in the hotter half of the slot and downward motion in the cooler half. It has been shown (Gershuni 1953; Rudakov 1967; Vest & Arpaci 1969; Korpela, Gozum & Baxi 1973) that the flow is unstable to travelling waves for fluids of Prandtl number $\sigma > 12.7$ and to stationary cells for $\sigma < 12.7$. The importance of travelling waves at high Prandtl numbers was first noted by Gill & Kirkham (1970) who showed that the critical value of the Rayleigh number A (based on slot width) is

$$A_{\mathrm{T}} \sim 9.4 \times 10^3 \, \sigma^{\frac{1}{2}} \quad (\sigma \to \infty). \tag{1.1}$$

The critical value for stationary instability in the form of transverse rolls is

$$A_{\mathrm{S}} \sim 7.9 \times 10^3 \, \sigma, \tag{1.2}$$

a result that appears to be valid to within a few percent for all Prandtl numbers. Although it has not been verified by asymptotic analysis as $\sigma \to \infty$, which would involve a critical-layer structure on the cavity centreline, Vest & Arpaci (1969) have established it numerically for values of σ as high as 10^3. The result (1.2) is of crucial significance in the description of the base flow in the vertical slot, for when $A > A_{\mathrm{S}}$ the conductive core solution will be destroyed by an imperfect bifurcation associated with the penetration of cells from the end zones of the slot; for $\sigma > 12.7$ stability

is lost to a time-dependent state at an even lower value of A. In either case, the complexities of the resulting flow pattern at supercritical values of A are difficult to treat analytically except in the neighbourhood of the critical value where the nonlinearity is weak; the stationary transverse rolls which appear at A_S are an integral part of the solution which allow the endwall boundary conditions to be satisfied (Daniels 1985*a*) and so cannot be ignored even in the computation of the base flow.

Despite these considerations, experiments by Elder (1965) clearly demonstrate the existence of a convective regime free from multiple-cell motions. For the high-Prandtl-number fluids used in the experiments, the critical Rayleigh numbers A_S and A_T are very large, and the onset of the convective regime produced by the expansion of the end-zones into the core of the slot as A increases (Daniels 1985*a*), can occur before either of the conditions (1.1) or (1.2) is met. In mathematical terms the simplest and most relevant model is one for which the Prandtl number is infinite, an assumption that is used as the basis for the present study; according to (1.1) and (1.2) the conductive solution is then completely stable. There is evidence (Elder 1966) that in many respects the resulting solution remains a good approximation at large and even moderate Prandtl numbers. The convective regime, where A is of order h, was first identified experimentally by temperature data obtained from interferometric measurements in air (Eckert & Carlson 1961) and carbon dioxide (Mordchelles-Regnier & Kaplan 1963), and it was later that Elder (1965) obtained more extensive velocity and temperature measurements for high-Prandtl-number oils. He also proposed a theoretical description of the flow based on the assumption of a uniform non-zero vertical temperature gradient β and valid, in an approximate sense, near mid-cavity height. This has subsequently been used as the base flow for stability analyses of the convective regime by Birikh *et al.* (1969), Gill & Kirkham (1970), Hart (1971), Mizushima & Gotoh (1976) and Bergholz (1978). For high-Prandtl-number fluids the core flow destabilizes into vertically stacked transverse rolls and this complicates the description of the development of the boundary-layer regime as $A/h \rightarrow \infty$. The formation of thin layers adjacent to each vertical wall of the cavity, and which contain most of the vertical mass flux, is suggested by Elder's approximate theoretical solution. Gill (1966) later developed a more complete asymptotic structure for the boundary-layer regime in which the core flow is vertically stratified and consists of a two-way horizontal shear flow entrained and detrained by the vertical boundary layers. Further studies of this regime and its stability have been made by Gill & Davey (1969), Blythe, Daniels & Simpkins (1983) and Daniels (1985*b*).

Numerical simulation of the full cavity flow at particular points in the three-dimensional parameter space (A, h, σ) has proved the most popular method of solution in recent years and many of the experimentally observed phenomena have been reproduced. Solutions mainly concerned with the vertical-slot limit ($h \gg 1$) have been obtained by Elder (1966), Catton, Ayyoswamy & Clever (1974), De Vahl Davis & Mallinson (1975), Seki, Fukusako & Inaba (1978), Bontoux & Roux (1982) and Lee & Korpela (1983). The aim of the present work is to obtain solutions of more general validity by utilizing the asymptotic structure of the flow. The contents of the paper are as follows. The governing equations and boundary conditions are stated in §2 and the asymptotic structure of the solution in the convective regime is obtained in §3. This leads to a simplified form of the governing equations in the core region of the slot and the novel problem of solving the vertical boundary-layer equations in a rectangle, subject to certain conditions on each of the four boundaries. Because of

the asymptotic representation and the assumption of large Prandtl number this problem contains only one parameter,

$$l = (A/h)^{\frac{1}{2}}, \tag{1.3}$$

which may be interpreted as a scaled horizontal aspect ratio (see (3.3) below). For very tall cavities ($l \to 0$) the conductive regime is recovered while the opposite limit ($l \to \infty$) corresponds to the boundary-layer regime. Numerical solutions are obtained for various values of l using a spectral decomposition in the vertical direction (§4). The results are described in §5 and a comparison is made with both the conductive solution and Elder's approximate solution. At large values of l ($l \geqslant l_c$ where $l_c \approx 11$) the solution is found to enter an unstable region (§6) where reliable numerical results are much more difficult to obtain. The presence of this region is confirmed by a stability analysis of the reduced equations and the threshold at l_c seems to be in good agreement with the observed onset of instability in experimental work. The results are discussed in §7.

2. Formulation

Fluid of density ρ, kinematic viscosity ν, thermal diffusivity κ and coefficient of thermal expansion α^* is contained in a two-dimensional vertical slot $0 \leqslant x^* \leqslant l^*$, $0 \leqslant z^* \leqslant h^*$ and is set into motion by maintaining the rigid vertical walls at different constant temperatures T_0^* and $T_0^* + \Delta T^*$. The horizontal walls are assumed to be rigid and perfectly insulated. The equations that govern the steady two-dimensional motion of the fluid in the Boussinesq approximation can be written in a convenient non-dimensional form as

$$\frac{\partial \overline{u}}{\partial \overline{x}} + \frac{\partial \overline{w}}{\partial \overline{z}} = 0, \tag{2.1}$$

$$\sigma^{-1}\left(\overline{u}\frac{\partial \overline{u}}{\partial \overline{x}} + \overline{w}\frac{\partial \overline{u}}{\partial \overline{z}}\right) = -\frac{\partial \overline{p}}{\partial \overline{x}} + \nabla^2 \overline{u}, \tag{2.2}$$

$$\sigma^{-1}\left(\overline{u}\frac{\partial \overline{w}}{\partial \overline{x}} + \overline{w}\frac{\partial \overline{w}}{\partial \overline{z}}\right) = -\frac{\partial \overline{p}}{\partial \overline{z}} + \nabla^2 \overline{w} + R\overline{T}, \tag{2.3}$$

$$\overline{u}\frac{\partial \overline{T}}{\partial \overline{x}} + \overline{w}\frac{\partial \overline{T}}{\partial \overline{z}} = \nabla^2 \overline{T}, \tag{2.4}$$

where $\nabla^2 = \partial^2/\partial \overline{x}^2 + \partial^2/\partial \overline{z}^2$. The coordinates $\overline{x}$, $\overline{z}$, velocity components $\overline{u}$, $\overline{w}$ and reduced pressure $\overline{p}$ have been made dimensionless by the quantities h^*, κ/h^* and $\rho\kappa\nu/h^{*2}$ respectively, while the temperature field T^* is expressed as

$$T^* = T_0^* + \Delta T^* \overline{T}. \tag{2.5}$$

The governing parameters in this formulation are the Prandtl number $\sigma = \nu/\kappa$, the Rayleigh number based on the slot height,

$$R = \frac{\alpha^* g^* \Delta T^* h^{*3}}{\kappa\nu}, \tag{2.6}$$

where g^* is the acceleration due to gravity, and the horizontal aspect ratio

$$L = l^*/h^*. \tag{2.7}$$

A stream function $\overline{\psi}$ is introduced, where

$$\overline{u} = \frac{\partial \overline{\psi}}{\partial \overline{z}}, \quad \overline{w} = -\frac{\partial \overline{\psi}}{\partial \overline{x}}. \tag{2.8}$$

The boundary conditions on the vertical walls of the slot are then

$$\left.\begin{aligned} &\overline{\psi} = \frac{\partial \overline{\psi}}{\partial \overline{x}} = 0 \quad (\overline{x} = 0, \overline{x} = L), \\ &\overline{T} = 0 \quad (\overline{x} = 0), \quad \overline{T} = 1 \quad (\overline{x} = L), \end{aligned}\right\} \tag{2.9}$$

while on the horizontal endwalls

$$\overline{\psi} = \frac{\partial \overline{\psi}}{\partial \overline{z}} = \frac{\partial \overline{T}}{\partial \overline{z}} = 0 \quad (\overline{z} = 0, \overline{z} = 1). \tag{2.10}$$

The present theory is concerned primarily with the infinite-Prandtl-number limit where the nonlinear inertia terms can be ignored in (2.2) and (2.3). Elimination of the pressure then yields the governing equations

$$\nabla^4 \overline{\psi} = R \frac{\partial \overline{T}}{\partial \overline{x}}, \tag{2.11}$$

$$\nabla^2 \overline{T} = \frac{\partial(\overline{T}, \overline{\psi})}{\partial(\overline{x}, \overline{z})}. \tag{2.12}$$

These equations, together with the boundary conditions (2.9) and (2.10) have solutions which possess the property of centro-symmetry (Gill 1966)

$$\overline{\psi}(\overline{x}, \overline{z}) = \overline{\psi}(L-\overline{x}, 1-\overline{z}), \quad \overline{T}(\overline{x}, \overline{z}) = 1-\overline{T}(L-\overline{x}, 1-\overline{z}), \tag{2.13}$$

so that in general only one half of the flow domain need be considered.

An alternative formulation based on the vertical aspect ratio

$$h = h^*/l^* = L^{-1}, \tag{2.14}$$

together with the horizontal Rayleigh number

$$A = \frac{\alpha^* g^* \Delta T^* l^{*3}}{\kappa \nu} = RL^3, \tag{2.15}$$

is particularly appropriate in the conductive limit, and the connection formulae (2.14), (2.15) can also be used to link the present results with those of other studies where required.

3. Asymptotic structure of the convective regime

When the vertical aspect ratio h is large and $A = RL^3$ is order one, the exact conductive solution of (2.11) and (2.12) is

$$\overline{T} = \tilde{x}, \quad \overline{\psi} = \tfrac{1}{24} A \tilde{x}^2 (1-\tilde{x})^2 \quad (0 \leqslant \tilde{x} \leqslant 1), \tag{3.1}$$

where $\tilde{x} = \overline{x}/L$, and is valid in the core region $0 < \overline{z} < 1$. Near the horizontal endwalls $\overline{z} = 0$ and $\overline{z} = 1$ the vertical two-way flow is turned in roughly square end zones. Here the flow is nonlinear (unless $A \ll 1$) and is generated by the requirement that the solution for $\overline{\psi}$ in (3.1) must be reduced to zero at the endwall. The properties of the

flow have been discussed by the present author (1985*a*) where it is shown that in the infinite-Prandtl-number limit, a consistent passive solution (i.e. that matches with (3.1)) can be found for all values of A. The imperfect bifurcation associated with the stationary conductive instability is avoided and as $A \to \infty$ a more gradual penetration occurs in which the end-zone spreads into the core on the vertical scale $\bar{z} \sim LA = A/h$. Thus the conductive solution is eventually destroyed throughout the slot when A is of order h, or more precisely, when

$$A/h \gtrsim 645 \tag{3.2}$$

(Daniels 1985*a*) and this provides a criterion for the onset of the convective regime.

An appropriate convective parameter l is defined by (1.3), so that

$$L = R^{-\frac{1}{4}} l \tag{3.3}$$

and l may be interpreted as a scaled horizontal aspect ratio. The present theory is based on the limit $R \to \infty$ with l finite, and is therefore restricted basically to tall slots. In finite-aspect-ratio cavities ($L = O(1)$) the convective regime corresponds to $R = O(1)$ and no simplification of the governing equations is possible; however, for $R \gg 1$ the boundary-layer structure proposed by Gill (1966) is contained (to leading order) within that considered here, so that the limit of the present theory as $l \to \infty$ may be of relevance to the boundary-layer regime in cavities of finite aspect ratio. It should be added, however, that a consistent horizontal boundary-layer structure has not yet been found for that situation, and it is not clear how the end-structure associated with the conductive regime adjusts as L increases to values of order one.

In the convective regime, where l is of order one, appropriate scalings for the core solution as $R \to \infty$ are

$$\overline{T} = T(x,z) + \ldots, \quad \overline{\psi} = R^{\frac{1}{4}} \psi(x,z) + \ldots, \tag{3.4}$$

where

$$\bar{x} = R^{-\frac{1}{4}} x, \quad \bar{z} = z. \tag{3.5}$$

From (2.11) and (2.12) the core region $0 \leqslant x \leqslant l$, $0 < z < 1$ is then governed by the vertical boundary-layer equations

$$\frac{\partial^4 \psi}{\partial x^4} = \frac{\partial T}{\partial x}, \quad \frac{\partial^2 T}{\partial x^2} = \frac{\partial (T, \psi)}{\partial (x, z)}. \tag{3.6}$$

These must be solved subject to the boundary conditions

$$\left.\begin{aligned} &\psi = \frac{\partial \psi}{\partial x} = 0 \quad (x = 0, x = l), \\ &T = 0 \quad (x = 0), \quad T = 1 \quad (x = l), \end{aligned}\right\} \tag{3.7}$$

on the vertical walls. At $z = 0$ and $z = 1$ the full conditions (2.10) cannot be satisfied because the highest derivatives in z do not appear in the reduced equations (3.6). Solutions of the vertical boundary-layer equations by approximate integral and Oseen techniques described by Blythe & Simpkins (1977) and Gill (1966) can be made to satisfy

$$\psi = 0 \quad (z = 0, z = 1), \tag{3.8}$$

and while it is not clear that the exact solution of (3.6), (3.7) has the same property, it is now shown that asymptotic forms exist for general values of l that are consistent with (3.8).

In view of the centro-symmetry property only the asymptotic structure near $z = 0$ need be considered and the results follow the pattern of the vertical boundary-layer

analysis of Blythe *et al.* (1983). As $z \to 0$ the solution divides laterally into five distinct zones. Near the hot wall, where $S = (l-x)/z^{\frac{1}{4}} = O(1)$, there is a Goldstein (1938, p. 638) region where the main temperature adjustment occurs. Thus

$$T \sim g(S), \quad \psi \sim z^{\frac{3}{4}} f(S) \quad \text{as } z \to 0, \tag{3.9}$$

where $g = -f'''$ and

$$f^{\mathrm{V}} + \tfrac{3}{4} f f^{\mathrm{IV}} = 0; \quad f = f' = 0, \quad f''' = -1 \quad (S = 0), \quad f'' \to 0 \quad (S \to \infty). \tag{3.10}$$

This system has previously been considered by Kuiken (1968). The solution has the limiting behaviour $f \sim A_1 S + A_0$ as $S \to \infty$, where $A_1 = 1.021$ and $A_0 = -0.738$, and the vertical velocity associated with A_1 generates a convection-dominated flow in an outer wall region where $\eta = (l-x)/z^{\frac{1}{10}} = O(1)$. Here

$$T \sim z^{\frac{3}{10}} G(\eta), \quad \psi \sim z^{\frac{3}{5}} F(\eta) \quad \text{as } z \to 0, \tag{3.11}$$

and it emerges from consideration of the solution near the cold wall that $G = KF^{\frac{1}{2}}$, where K is an arbitrary constant and

$$F''' + K(F^{\frac{1}{2}} - F^{\frac{1}{2}}(\infty)) = 0; \quad F(0) = 0, \quad F \to F(\infty) \quad (\eta \to \infty). \tag{3.12}$$

Setting $a_0 = F(\infty)$ the solution

$$T \sim b_0 z^{\frac{3}{10}}, \quad \psi \sim a_0 z^{\frac{3}{5}} \quad (z \to 0), \tag{3.13}$$

where

$$b_0 = K a_0^{\frac{1}{2}}, \tag{3.14}$$

is transmitted across the main core region $0 < x < l$ and at the cold wall, where $x = 0$, generates another convection-dominated zone where $\tilde{\eta} = x/z^{\frac{1}{10}} = O(1)$. Here

$$T \sim z^{\frac{3}{10}} \tilde{G}(\tilde{\eta}), \quad \psi \sim z^{\frac{3}{5}} \tilde{F}(\tilde{\eta}) \quad \text{as } z \to 0, \tag{3.15}$$

and $\tilde{G} = K\tilde{F}^{\frac{1}{2}}$, where

$$\tilde{F}''' - K(\tilde{F}^{\frac{1}{2}} - a_0^{\frac{1}{2}}) = 0; \quad \tilde{F}(0) = \tilde{F}'(0) = 0, \quad \tilde{F} \to a_0 \quad (\tilde{\eta} \to \infty). \tag{3.16}$$

The relation between $\tilde{F}$ and $\tilde{G}$, which in turn determines that between F and G, ensures that the temperature condition at the cold wall is satisfied; this requirement arises because a further inner layer, where $x/z^{\frac{1}{5}} = O(1)$ and the conductive term in the heat equation is significant, is found to have no influence on the leading-order behaviour near the wall determined by the solution of (3.16).

The main results (3.13) are seen to be consistent with (3.8) and to represent a flow at the temperature of the cold wall but with large horizontal velocity and vertical temperature gradient; the horizontal flow is due to the entrainment of fluid near the hot wall where there is a rapid rise in temperature. The value of K cannot be determined by the asymptotic analysis, although the solution of (3.12) gives

$$F'(0) = a_0^{\frac{5}{6}} K^{\frac{1}{3}} q_1, \tag{3.17}$$

where $q_1 = 0.834$, so that matching with $f'(\infty)$ requires that

$$a_0^{\frac{5}{6}} K^{\frac{1}{3}} = A_1/q_1. \tag{3.18}$$

Thus, making use of (3.14),

$$a_0 = B^{\frac{3}{5}} K^{-\frac{2}{5}}, \quad b_0 = B^{\frac{1}{5}} K^{\frac{4}{5}}, \tag{3.19}$$

where $B = (A_1/q_1)^3 = 1.832$. Presumably K is a function of l, and its indeterminacy reflects a dependence of the local solution on the global properties of the flow. Alternative structures near $z = 0$, corresponding to $K = 0$, in which the core region is isothermal near the end and the boundary-layer velocity $\psi_x \sim -A_1 z^{\frac{1}{2}}$ at the hot

wall drives an x-dependent core solution satisfying $\psi_{xxxx} = 0$, do not appear to be relevant, and probably imply the attainment of negative temperatures on the colder side. In the boundary-layer regime the structure discussed by Blythe *et al.* (1983) is equivalent to the limiting behaviour $K \to K_0$ as $l \to \infty$, where K_0 is a numerical constant, while consistency with the conductive regime requires that $K = O(l^{-\frac{1}{3}})$ as $l \to 0$. Further analysis suggests that the above solution can be matched to a horizontal boundary-layer structure that allows an adjustment to the full conditions (2.10). However, this is rather complicated and is discussed elsewhere (Daniels 1986). The present paper is concerned with the reduced core problem and the behaviour of its solution for different values of the convective parameter l. It should be noted that conditions of the form (3.8) preclude the exact solution (3.1).

4. Spectral decomposition and numerical solution

Some numerical solutions of the reduced system (3.6)–(3.8) were sought by means of the spectral decomposition

$$T = z + \sum_{n=1}^{\infty} a_n(x) \sin n\pi z, \quad \psi = \sum_{n=1}^{\infty} b_n(x) \sin n\pi z. \tag{4.1}$$

The precise status of this representation is not clear, but if the structure outlined in §3 is relevant, the fact that each of the functions $T-z$ and ψ vanishes at $z = 0$ and $z = 1$ and has a z-derivative that is absolutely integrable from $z = 0$ to $z = 1$, validates the use of the sine series (4.1). In particular it allows the term-by-term differentiation needed in the representation of the z-derivatives in the heat equation (see, for example, Tolstov 1962, pp. 75, 137). Substitution of (4.1) into (3.6) and truncation at $n = N$ leads to a set of ordinary differential equations

$$b_n^{\mathrm{IV}} = a_n', \quad a_n'' + b_n' = \phi_n^N, \quad (n = 1, 2, \ldots, N), \tag{4.2}$$

for the coefficients a_n and b_n, where ϕ_n^N is a nonlinear function of a_m, a_m', b_m, b_m' $(m = 1, 2, \ldots, N)$ representing the contribution of terms proportional to $\sin n\pi z$ arising from the product of the two series on the right-hand side of the heat equation. Details of the evaluation of ϕ_n^N are given by Daniels & Simpkins (1982).

At the cold wall, the boundary conditions (3.7) require that

$$a_n = 2(-1)^n/n\pi, \quad b_n = b_n' = 0 \quad (x = 0), \tag{4.3}$$

while the three remaining conditions are obtained from considerations of centro-symmetry. This avoids the computation of the flow in $\frac{1}{2}l < x \leqslant l$ and, from (2.13), implies that

$$\psi(x, z) = \psi(l-x, 1-z), \quad T(x, z) = 1 - T(l-x, 1-z). \tag{4.4}$$

From (4.1) this is equivalent to the requirement that if n is odd

$$a_n = b_n' = b_n''' = 0 \quad \text{on } x = \tfrac{1}{2}l, \tag{4.5}$$

while if n is even

$$a_n' = b_n = b_n'' = 0 \quad \text{on } x = \tfrac{1}{2}l, \tag{4.6}$$

and in either case this completes the six boundary conditions needed to solve (4.2).

Since $\phi_1^1 = 0$ an analytical solution is possible for the single-mode system obtained

n_0	$\psi(\frac{1}{2}l,\frac{1}{2}) = \sum_{n\,\mathrm{odd}}^{n_0}(-1)^{(n-1)/2}b_n(\frac{1}{2}l)$	$\frac{\partial T}{\partial z}(\frac{1}{2}l,\frac{1}{2}) = 1+\pi\sum_{n\,\mathrm{even}}^{n_0-1}(-1)^{n/2}na_n(\frac{1}{2}l)$
1	0.6547	1
3	0.5467	0.3270
5	0.5935	0.9041
7	0.5674	0.3989
9	0.5835	0.8436
11	0.5731	0.4521
13	0.5799	0.7965
15	0.5755	0.4942
17	0.5783	0.7594
19	0.5764	0.5219

TABLE 1. Convergence of the Fourier series for ψ and $\partial T/\partial z$ at the centre of the slot, with $l = 8$ and $N = 20$: the partial sums of the series are shown. Increments of the Newton iteration are within a pre-relaxation tolerance of 3×10^{-5}.

when $N = 1$, and this provides an initial guess for the computation of the solution at higher truncation levels. The solution is given by

$$\left.\begin{aligned} b_1 &= C+C_+\cosh\frac{X}{\sqrt2}\cos\frac{X}{\sqrt2}+C_-\sinh\frac{X}{\sqrt2}\sin\frac{X}{\sqrt2},\\ a_1 &= \frac{1}{\sqrt2}\left\{(C_--C_+)\sinh\frac{X}{\sqrt2}\cos\frac{X}{\sqrt2}-(C_-+C_+)\cosh\frac{X}{\sqrt2}\sin\frac{X}{\sqrt2}\right\}, \end{aligned}\right\} \tag{4.7}$$

where $X = x-\frac{1}{2}l$,

$$C_\pm = -\frac{\sqrt2}{\pi c}\left(\cosh\frac{l}{2\sqrt2}\sin\frac{l}{2\sqrt2}\pm\sinh\frac{l}{2\sqrt2}\cos\frac{l}{2\sqrt2}\right), \tag{4.8}$$

$$C = \frac{1}{\sqrt2\pi c}\left(\sinh\frac{l}{\sqrt2}+\sin\frac{l}{\sqrt2}\right), \tag{4.9}$$

and $c = \sinh^2(l/2\sqrt2)+\sin^2(l/2\sqrt2)$. The solution for higher values of N was obtained using Newton's method to predict new values of the variables a_n, b_n at each stage of an iterative scheme. The equations were reduced to first-order form by introducing additional variables and discretized using central differences in the x-direction. The Newton increments for the nth mode were calculated by a Gauss–Seidel technique regarding all other modes as fixed at their most recently computed values. The new values were then also subjected to a relaxation before the next higher mode was calculated. The overall procedure consisted of setting $N = 2$ with (4.7) and $a_2 = b_2 = 0$ as initial guesses, obtaining reasonable convergence at this level and then increasing N using the previously calculated modes, along with $a_N = b_N = 0$, as new initial guesses. Most solutions were computed with maximum truncation levels $N = 20$ or 30, and 20 steps across the half-slot width. Tests with 10 and 40 steps indicated that for moderate values of l this step size produced an error of less than $\frac{1}{2}\%$ in the value of ψ at the centre of the slot. At high truncation levels it was found necessary to use quite severe under-relaxation, as in the vertical boundary-layer calculations described by Blythe *et al.* (1983).

Tables 1 and 2 contain information concerning the convergence of the Fourier series and the effect of the truncation. The slow decay of $a_n(0)$ with n, as given by (4.3), is associated with the discontinuity in T at $x = 0$, $z = 1$ (indeed, term-by-term

N	$b_1(\frac{1}{2}l)$	$a_2(\frac{1}{2}l)$	$b_3(\frac{1}{2}l)$	$a_4(\frac{1}{2}l)$	$\psi(\frac{1}{2}l, \frac{1}{2})$	Δ
1	0.4850	—	—	—	0.4850	10^{-6}
5	0.6211	0.0929	0.0692	0.0306	0.5524	10^{-6}
10	0.6446	0.1029	0.0984	0.0418	0.5741	10^{-6}
20	0.6547	0.1071	0.1080	0.0459	0.5764	3×10^{-5}
30	0.6581	0.1085	0.1109	0.0471	0.5796	5×10^{-4}

TABLE 2. Convergence of the solution as a function of truncation level N for $l = 8$. Δ is the pre-relaxation tolerance of the increments of the Newton iteration.

differentiation of the series for T is not valid at $x = 0$) and this generally leads to a very slow convergence of the Fourier series for $\partial T/\partial z$ and $\partial\psi/\partial z$ when $x > 0$. In the circumstances, the convergence of the series for the basic functions T and ψ was found to be remarkably good, and estimates of $\partial T/\partial z$ can be obtained either graphically from T or by extrapolation based on the mean of the partial sums of the series for $\partial T/\partial z$ (see table 1).

5. Results for the stable region $l < l_c$

At low values of the convective parameter ($l = 2$, 4, figure 1) the numerical results exhibit a Gibbs phenomenon caused by the regions of rapid adjustment near the endwalls at $z = 0$ and $z = 1$ which characterize the conductive regime. These have a vertical scaling proportional to l^4 as $l\to0$. Away from the endwalls the conductive core solution

$$T \sim \frac{x}{l}, \quad \psi \sim \tfrac{1}{24}l^3\left(\frac{x}{l}\right)^2\left(1-\frac{x}{l}\right)^2 \quad (l \ll 1), \tag{5.1}$$

is accurately reproduced (figures 1–3). As l increases from 4 to 6 there is a rapid rise of the vertical temperature gradient in the slot, associated with the onset of the convective regime (figure 4), and at $l = 8$ the streamline and isotherm patterns (figure 3*b*) indicate significant horizontal motion and a strong vertical stratification on the centreline of the slot. It was found that results exhibiting clear convergence could be obtained for values of l as high as 11, where the stream function at the centre of the slot appears to approach a maximum value (figure 5). The vertical temperature gradient at the same position reaches a maximum at about $l = 6.5$, and thereafter the maximum gradient on $z = \frac{1}{2}$ moves to equal and opposite locations closer to each vertical wall (figure 6). Thus a vertical gradient averaged over the width of the slot is subject to significantly less variation than that of figure 4. Figure 7 shows the variation of the Nusselt number representative of the heat transfer out of the cold wall. This is defined by

$$\overline{Nu} = \frac{1}{\Delta T^*}\int_{z^*-0}^{z^*-h^*}\left.\frac{\partial T^*}{\partial x^*}\right|_{x^*-0} \mathrm{d}z^* = R^{\frac{1}{4}}Nu, \tag{5.2}$$

where

$$Nu = \int_0^1 \left.\frac{\partial T}{\partial x}\right|_{x-0} \mathrm{d}z. \tag{5.3}$$

In the conductive limit, $Nu \sim l^{-1}$ as $l\to0$, from (5.1).

Asymptotes for the boundary-layer limit ($l\to\infty$) are also shown in figures 4, 5 and 7. These are the values predicted by a solution of the vertical boundary-layer

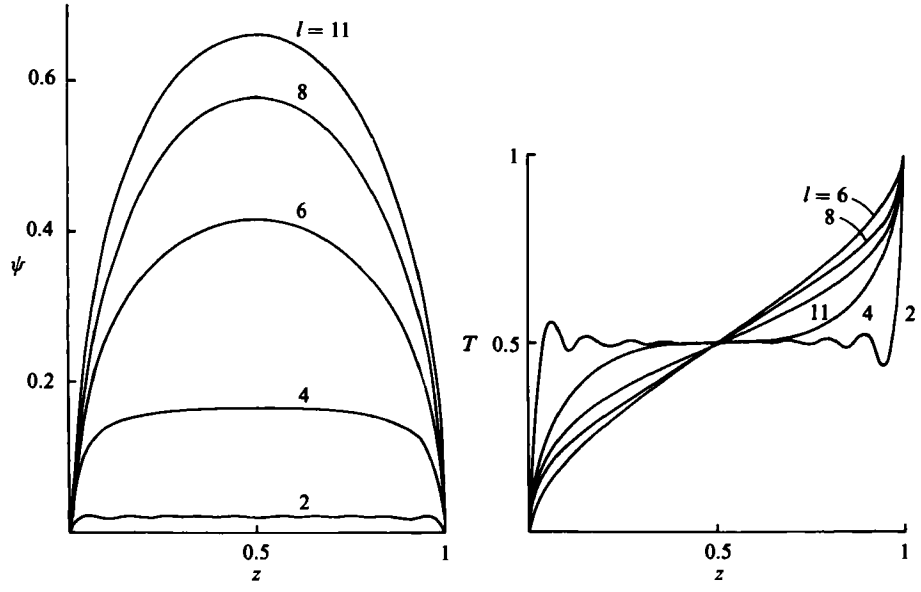

FIGURE 1. Stream function and temperature profiles on the centreline of the slot, $x = \frac{1}{2}l$, for $l = 2, 4, 6, 8, 11$.

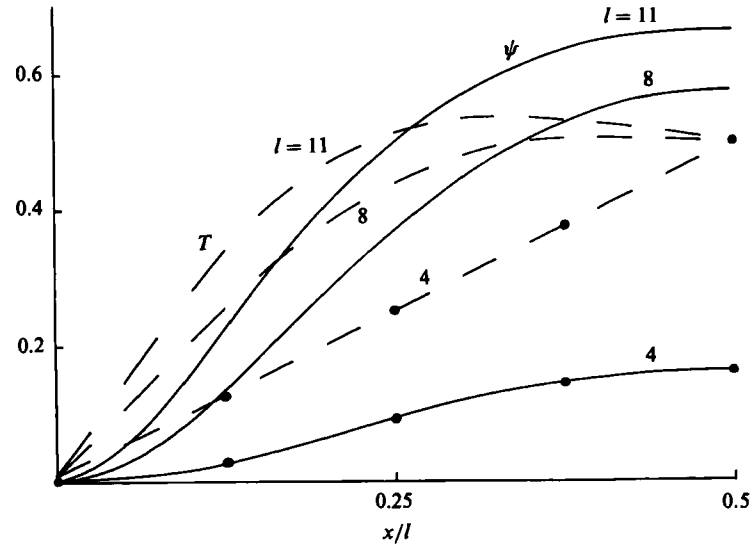

FIGURE 2. Stream function (——) and temperature (– – –) profiles at mid-cavity level, $z = \frac{1}{2}$, for $l = 4, 8, 11$. Conductive solution for $l = 4$ also shown (●).

equations using a numerical method similar to that described here and reported by Blythe *et al.* (1983). The main difference is that the vertical profiles of stream function and temperature are required to approach x-independent forms at the edge of the layer. Thus the boundary conditions (4.5) and (4.6) are replaced appropriately and the solution is obtained using an artificial outer boundary at $x = x_\infty$; the asymptotes shown in the figures are for $x_\infty = 8$. It has not been possible to obtain solutions for

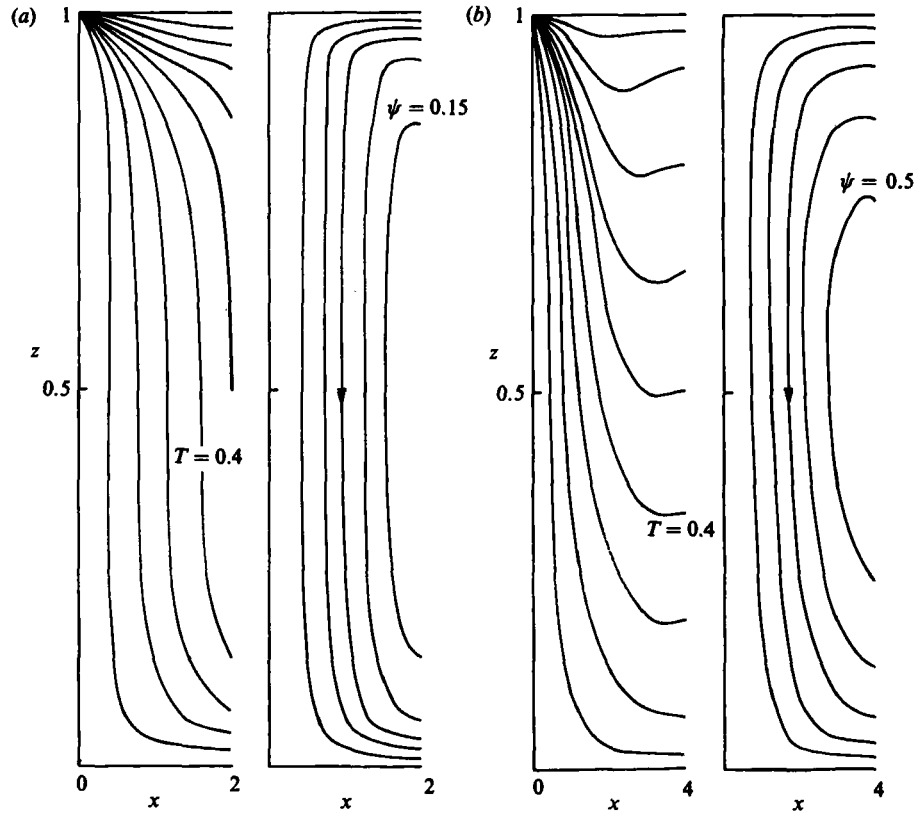

FIGURE 3. Streamline and isotherm patterns for (*a*) $l = 4$ ($\Delta T = 0.1$, $\Delta\psi = 0.03$), (*b*) $l = 8$ ($\Delta T = 0.1$, $\Delta\psi = 0.1$). Half the slot is shown in each case.

larger values of x_∞ (e.g. $x_\infty = 12$) due to stability problems (see also below) although the value $x_\infty = 8$ is at least large enough for the oscillatory decay of the boundary-layer solution (cf. (5.14) below) to be identified; furthermore the results agree well with numerical and experimental evidence (see Blythe *et al.* 1983). In figure 4, experimental measurements of the vertical temperature gradient at the centre of the slot are seen to overshoot their limiting values, consistent with the present calculations, while in figure 8 a comparison of the vertical velocity profile at $l = 11$ with that obtained experimentally by Elder (1965) at a comparable value of l indicates excellent agreement.

Further results shown in figures 5 and 8 give a comparison with an approximate solution obtained by Elder (1965). This solution is based on the neglect of the horizontal velocity component and therefore, it is argued, is most relevant near mid-cavity level, $z = \frac{1}{2}$. The solution is written

$$T = \beta(z-\tfrac{1}{2}) + \tilde{T}(x), \quad \psi = \tilde{\psi}(x), \tag{5.4}$$

where β is the (externally specified) vertical temperature gradient; this constant gradient may be compared with the real x-variation evident in figure 6. Substitution into the governing equations (3.6) gives

$$\tilde{\psi}^{\mathrm{IV}} = \tilde{T}', \quad \tilde{T}'' + \beta\tilde{\psi}' = 0, \tag{5.5}$$

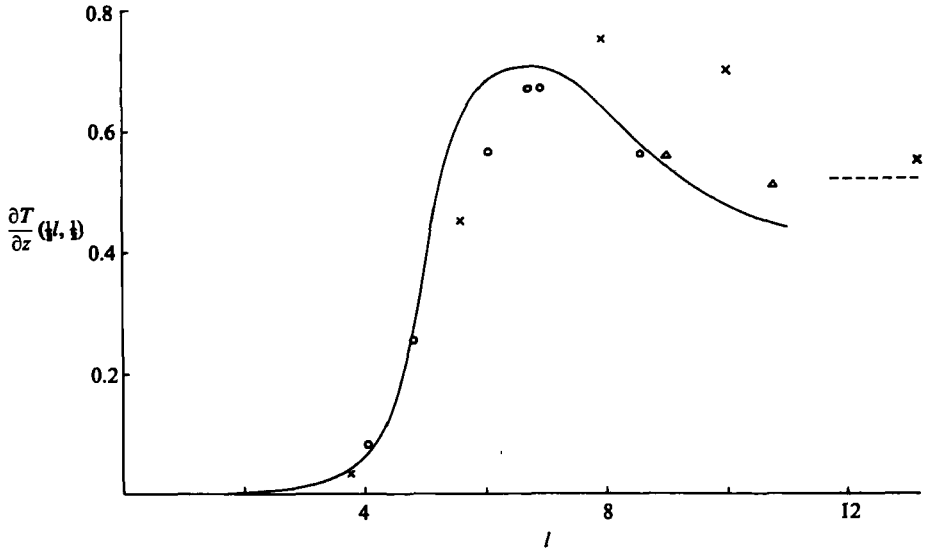

FIGURE 4. The vertical temperature gradient at the centre of the slot as a function of l. The broken curve is the large-l asymptote obtained by Blythe *et al.* (1983); the gradient is expected to be exponentially small in the conductive limit ($l \to 0$). Experimental results are due to Hart (1971) ○, $h = 37$, $\sigma = 6.7$. Numerical results due to Elder (1966) ×, $h = 1$, $\sigma = 1$, and Lee & Korpela (1983) △, $h = 15$, $\sigma = 20$ are also shown.

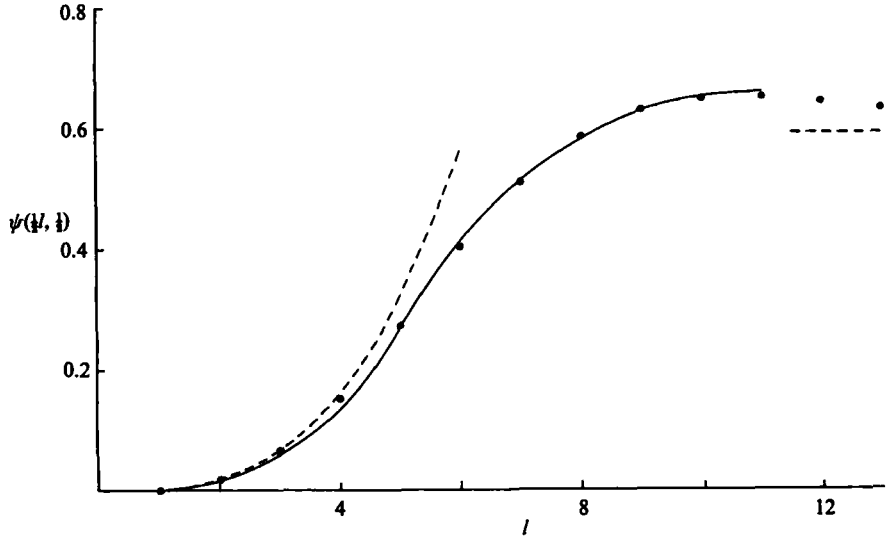

FIGURE 5. The stream function at the centre of the slot as a function of the convective parameter l. Broken curves show asymptotes based on the conductive solution (5.1) ($l \to 0$) and the boundary-layer calculations of Blythe *et al.* (1983) ($l \to \infty$). The approximate theoretical solution (5.12) for $\beta = \frac{1}{2}$ is also shown (●).

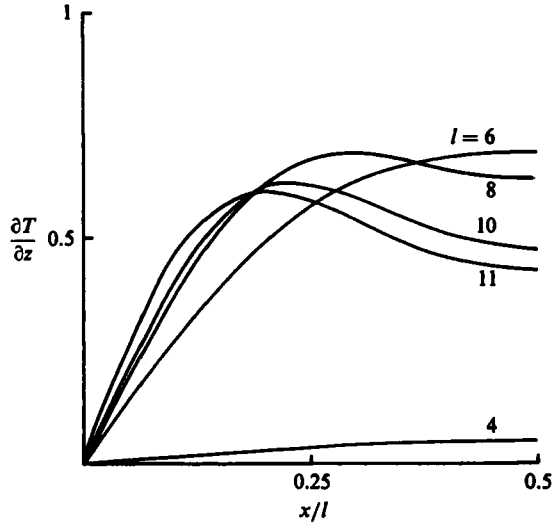

FIGURE 6. The vertical temperature gradient profile at mid-cavity level, $z = \frac{1}{2}$, for $l = 4, 6, 8, 10, 11$.

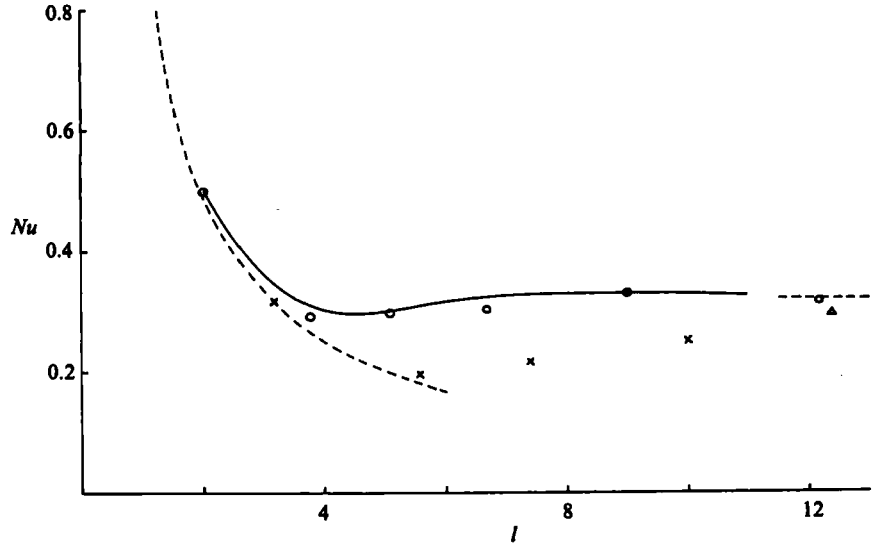

FIGURE 7. The Nusselt number Nu as a function of l. Broken curves show asymptotes based on the conductive solution (5.1) ($l \to 0$) and the boundary-layer calculations of Blythe *et al.* (1983) ($l \to \infty$). Numerical results due to Catton *et al.* (1974) ○, $h = 15$, $\sigma = \infty$; Elder (1966) ×, $h = 1$, $\sigma = 1$; and Rubel & Landis (1969) △, $h = 5$, $\sigma = 2 \times 10^3$ are also shown.

and since $\tilde{\psi}$ must be even and $\tilde{T} - \frac{1}{2}$ odd about $x = \frac{1}{2}l$ the required solutions are

$$\tilde{T} - \tfrac{1}{2} = \Theta(\tilde{X}), \quad \tilde{\psi} = l^3 \Psi(\tilde{X}) \quad (-\tfrac{1}{2} \leqslant \tilde{X} \leqslant \tfrac{1}{2}), \tag{5.6}$$

where

$$\Psi(\tilde{X}) = \gamma^{-3}\{D + D_+ \cosh\gamma\tilde{X} \cos\gamma\tilde{X} + D_- \sinh\gamma\tilde{X} \sin\gamma\tilde{X}\}, \tag{5.7}$$

and

$$\Theta(\tilde{X}) = 2(D_- - D_+) \sinh\gamma\tilde{X} \cos\gamma\tilde{X} - 2(D_+ + D_-) \cosh\gamma\tilde{X} \sin\gamma\tilde{X}, \tag{5.8}$$

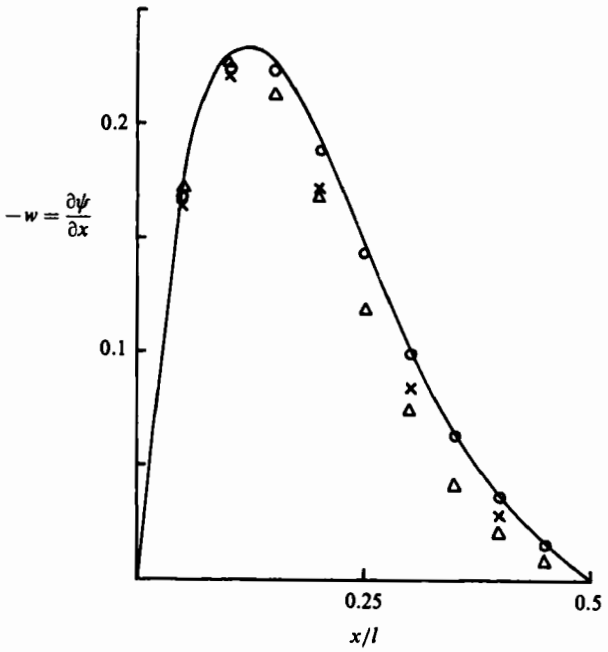

FIGURE 8. Vertical velocity profile at mid-cavity level, $z = \frac{1}{2}$, for $l = 11$. Experimental results due to Elder (1965) $\times$, $h = 18.6$, $A = 4 \times 10^5$ ($l \approx 12$), $\kappa = 1.05 \times 10^{-3}$, and the approximate theoretical solution (5.6) with $\beta = \frac{1}{2}$ for $l = 11$ ($\bigcirc$) and $l = 12$ ($\triangle$) are shown for comparison.

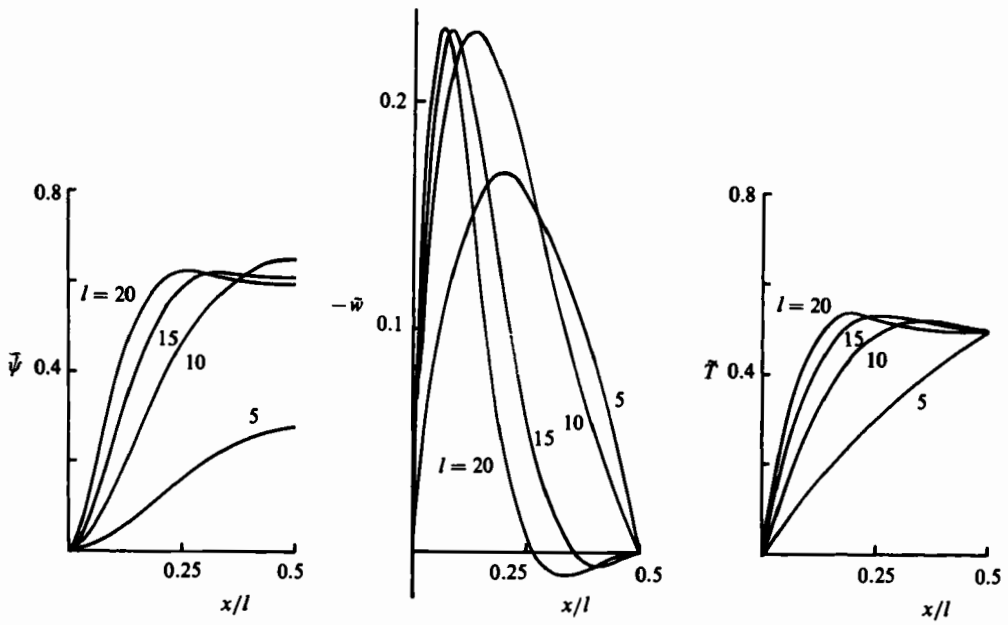

FIGURE 9. The base profiles $\tilde{\psi} = l^3\Psi$, $\mathrm{d}\tilde{\psi}/\mathrm{d}x = -\tilde{w} = l^2\Psi'$ and $\tilde{T} = \Theta + \frac{1}{2}$ as functions of x/l for various values of l with $\beta = \frac{1}{2}$. (The universal profiles Ψ, Ψ', Θ are easily obtained by replacing l with $2^{\frac{1}{2}}\gamma$.)

are dependent on the single parameter

$$\gamma = (\tfrac{1}{4}\beta)^{\frac{1}{4}} l = \left(\frac{A\beta}{4h}\right)^{\frac{1}{4}}, \tag{5.9}$$

and the normalized horizontal coordinate $\tilde{X} = X/l = (x-\frac{1}{2}l)/l$. The boundary conditions $\tilde{T} = \tilde{\psi} = \tilde{\psi}' = 0$ on $x = 0$ determine the three arbitrary constants in (5.7) and (5.8) as

$$D_{\pm} = -\frac{1}{8d}(\cosh\tfrac{1}{2}\gamma \sin\tfrac{1}{2}\gamma \pm \sinh\tfrac{1}{2}\gamma \cos\tfrac{1}{2}\gamma), \tag{5.10}$$

$$D = \frac{1}{16d}(\sinh\gamma + \sin\gamma), \tag{5.11}$$

where $d = \sinh^2\tfrac{1}{2}\gamma + \sin^2\tfrac{1}{2}\gamma$.

It is commonly assumed that $\beta = \frac{1}{2}$, this value being consistent with the experimental measurements made by Elder (1965). It is also in good agreement with the value 0.52 obtained by numerical solution of the vertical boundary-layer equations (Blythe *et al.* 1983) as well as numerical solutions of the full equations (e.g. Lee & Korpela 1983). The parameter γ is a combination of the vertical temperature gradient β and the convective parameter l; profiles of the approximate solution in figure 9 show the development from the conductive regime ($\gamma \to 0$) to the boundary-layer regime ($\gamma \to \infty$). According to this solution the value of the stream function at the centre of the slot is given from (5.6)–(5.11) as

$$\tilde{\psi}(\tfrac{1}{2}l) = l^3\Psi(0) = (4\beta)^{-\frac{3}{4}}\left\{\frac{\sinh\tfrac{1}{2}\gamma - \sin\tfrac{1}{2}\gamma}{\cosh\tfrac{1}{2}\gamma + \cos\tfrac{1}{2}\gamma}\right\}. \tag{5.12}$$

This is compared with the computed results in figure 5 for $\beta = \frac{1}{2}$. Note that

$$\tilde{\psi}(\tfrac{1}{2}l) \sim (4\beta)^{-\frac{3}{4}}(1 - 2e^{-\frac{1}{2}\gamma}\{\cos\tfrac{1}{2}\gamma + \sin\tfrac{1}{2}\gamma\}) \quad \text{as } \gamma \to \infty, \tag{5.13}$$

which predicts that $\tilde{\psi}(\frac{1}{2}l) \to 0.595$ when $\beta = \frac{1}{2}$. This value compares well with that of 0.59 predicted by the numerical solution of the vertical boundary-layer equations (Blythe *et al.* 1983). The approximation to the profile in the boundary layer near the cold wall obtained from (5.7) is

$$\tilde{\psi} \sim (4\beta)^{-\frac{3}{4}}(1 - e^{-\gamma\tilde{x}}\{\cos\gamma\tilde{x} + \sin\gamma\tilde{x}\}), \tag{5.14}$$

where $\tilde{x} = x/l$ and this predicts that $\tilde{\psi}$ has a first maximum as a function of x at $x = \pi l/\gamma = \pi(4/\beta)^{\frac{1}{4}}$ which is approximately 5.28 when $\beta = \frac{1}{2}$; this also compares well with the result obtained by Blythe *et al.* (1983, figure 5).

In summary the approximate theory with $\beta = \frac{1}{2}$ is seen to provide a surprisingly accurate estimate of the mid-cavity flow properties over a wide range of values of l. Although the vertical temperature gradient at the centre of the slot varies significantly from the value $\frac{1}{2}$ (figure 4), the good agreement is probably due to the proximity of this value to an averaged gradient across the width of the slot (figure 6).

6. The unstable region $l > l_c$

For $l \gtrsim 11$ the numerical calculations entered an unstable region where the addition of an extra mode (e.g. the 18th for $l = 12$ and the 9th for $l = 16$) resulted in an abrupt amplification from the single-cell solution into multiple-cell states of the type shown in figures 10 and 11. Although these solutions have Newton increments less than 10^{-2} (after many iterations) the convergence of the scheme and the effect of mode truncation could no longer be guaranteed with complete confidence. A different

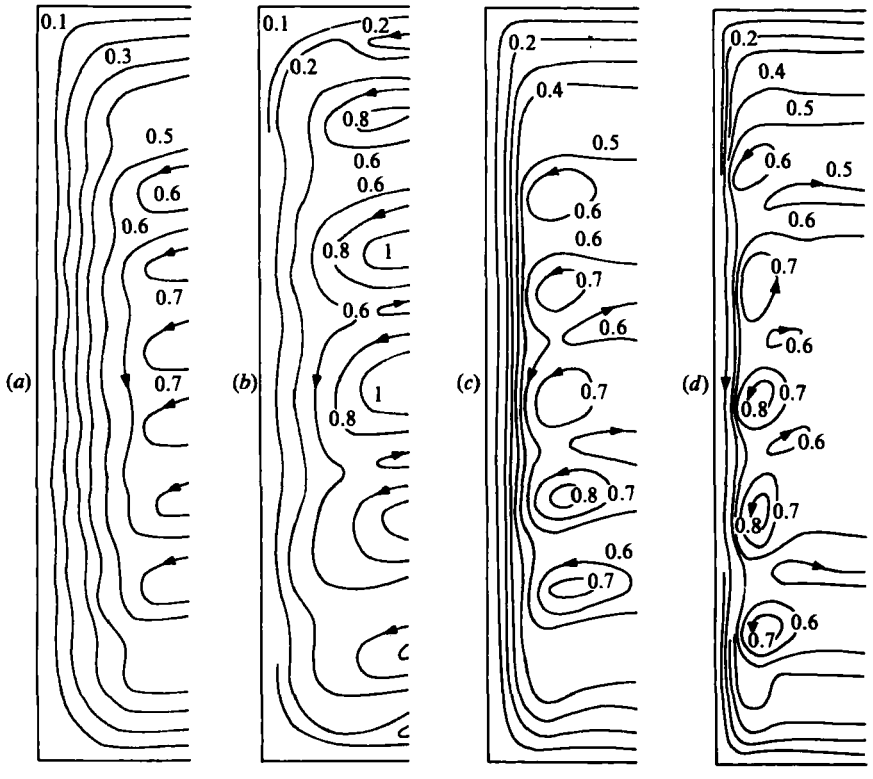

FIGURE 10. Streamlines of typical flow computations in the unstable region: (a) $l = 12$, (b) 16, (c) 24, (d) 40. Half the slot is shown in each case.

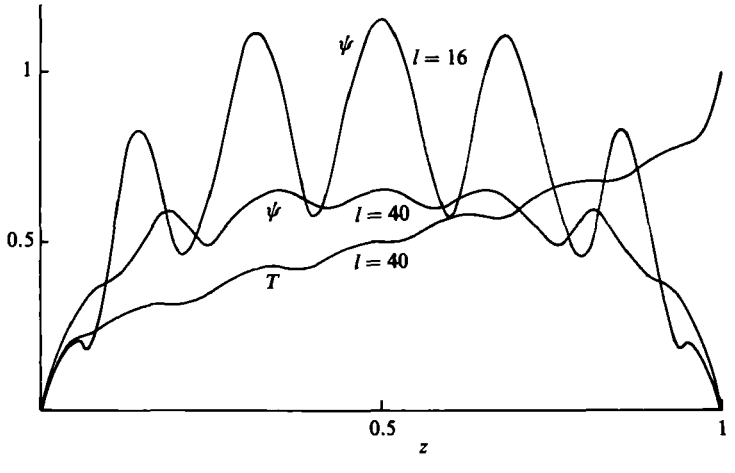

FIGURE 11. Stream function and temperature profiles on the centreline of the slot, $x = \frac{1}{2}l$, in the unstable region and corresponding to flow patterns shown in figure 10.

numerical approach may be needed to obtain accurate solutions in this region, but the sudden change in character of the solution and its possible connection with the observations of Elder (1965) and others seems worthy of note. It should be added that for sufficiently low truncations the roll instabilities are avoided, presumably due to the absence of the unstable vertical wavelengths. Thus clear convergence could

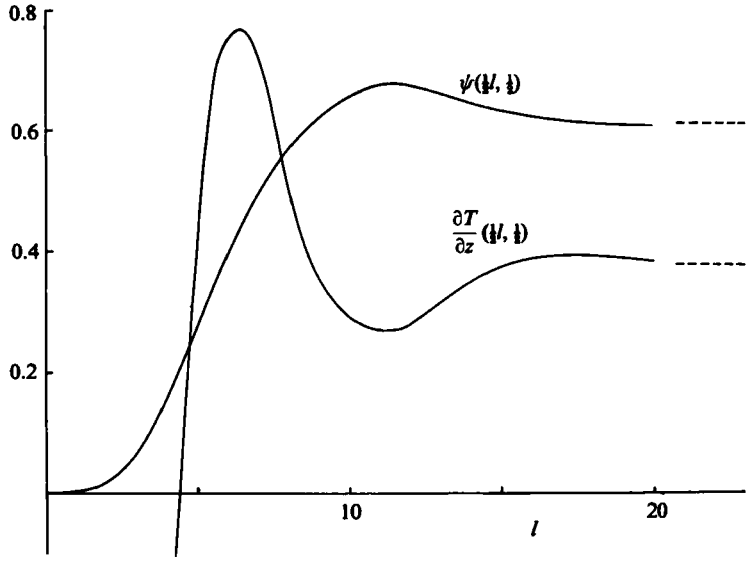

FIGURE 12. The stream function and vertical temperature gradient at the centre of the slot as functions of l for the truncation level $N = 3$. The broken lines show asymptotes predicted by a boundary-layer calculation with $x_\infty = 12$.

always be obtained when $N = 3$, and a single-cell circulation is produced for all values of l. In the conductive limit the behaviour of the vertical temperature gradient shown in figure 12 reflects the inadequacy of the truncated representation, but at higher values of l the results compare favourably with those of figures 4 and 5 and allow what may be a crude approximation to the single-cell solution to be traced into the boundary-layer regime ($l \to \infty$). Indeed, it was confirmed that the solution approaches that obtained by solving the boundary-layer equations in the region $0 \leqslant x \leqslant x_\infty$ with the assumption of appropriately symmetric, and x-independent core forms at x_∞. This is the problem solved by Blythe *et al.* (1983) with $x_\infty = 8$ although here, taking $N = 3$, it was found that stable solutions could be obtained with x_∞ as high as 12 or more.

Support for the existence of the critical point l_c of the reduced system (3.6)–(3.8) is provided by a stability analysis of the approximate base flow (5.4). At infinite Prandtl number travelling-wave solutions can be ignored (Gill & Kirkham 1970), and neutrally stable stationary solutions can be found by setting

$$\left.\begin{aligned} T &= \beta(z-\tfrac{1}{2})+\tfrac{1}{2}+\Theta(\bar{X})+\left\{\theta(\bar{X})\exp\left(\frac{\mathrm{i}\alpha z}{l^4}\right)+\text{c.c.}\right\}, \\ \psi &= l^3\Psi(\bar{X})+l^3\left\{\phi(\bar{X})\exp\left(\frac{\mathrm{i}\alpha z}{l^4}\right)+\text{c.c.}\right\}, \end{aligned}\right\} \tag{6.1}$$

where c.c. denotes complex-conjugate, α/l^4 is the wavenumber in the vertical direction and no account is taken of the boundary conditions at $z = 0$ and $z = 1$. Substitution into (3.6), (3.7) and linearization yields the stability equations

$$\phi^{\mathrm{IV}} = \theta', \quad \theta'' = \mathrm{i}\alpha(\Theta'\phi - \Psi'\theta) - 4\gamma^4\phi', \tag{6.2}$$

with

$$\phi = \phi' = \theta = 0 \quad \text{on } \bar{X} = \pm\tfrac{1}{2}. \tag{6.3}$$

Solutions for real values of α can be expressed in the form

$$\phi = \mathrm{e}^{\mathrm{i}k}(\phi_\mathrm{o}+\mathrm{i}\phi_\mathrm{e}), \quad \theta = \mathrm{e}^{\mathrm{i}k}(\theta_\mathrm{e}+\mathrm{i}\theta_\mathrm{o}), \tag{6.4}$$

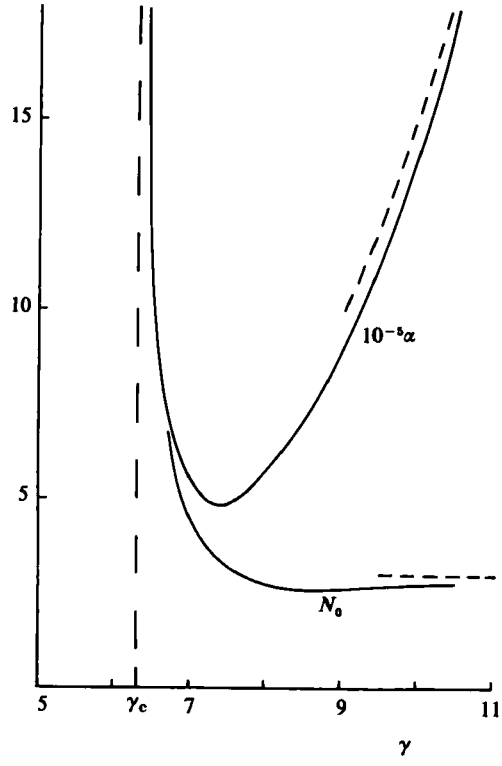

FIGURE 13. The wavenumber α, and the corresponding roll number $N_0 = \alpha/2\pi l^4 = \alpha\beta/8\pi\gamma^4$ for $\beta = \frac{1}{2}$, as functions of γ. The broken curves (– – –) are the asymptotes given by (6.18) and (6.20).

where k is an arbitrary constant, ϕ_o, ϕ_e, θ_o and θ_e are real functions of $\tilde{X}$ and the subscripts refer to even and odd solutions (see Vest & Arpaci 1969). However, the computation of three linearly independent solution pairs θ, ϕ from $\tilde{X} = -\frac{1}{2}$ to $\tilde{X} = \frac{1}{2}$ by a Runge–Kutta method and the location of the zeros of the 3×3 complex determinant formed from the boundary conditions at $\tilde{X} = \frac{1}{2}$ leads to the determination of α at a given value of γ in a straightforward manner. Real solutions for α are found to exist for $\gamma \geqslant \gamma_c \approx 6.3$ and are shown in figure 13. The behaviour $\alpha \to \infty$ as $\gamma \to \gamma_c +$ suggests that the point γ_c may be the critical point for the instability of shorter wavelengths $z = O(R^{-\frac{1}{4}})$ also. These are precluded within the context of the reduced system, which neglects rapid variations in the z-direction, but it seems likely that the present results provide the lower branch of a neutral stability curve in the (γ, α)-plane, possibly stemming from γ_c and with an upper branch corresponding to the short-wavelength instabilities. The neutral curve in figure 13 is consistent with the long-wavelength asymptote of solutions obtained by Bergholz (1978).

The critical point γ_c can be found by considering the limit $\alpha \to \infty$. An 'outer' solution is assumed in the form

$$\phi \sim \tilde{\phi}(\tilde{X}), \quad \theta \sim \tilde{\theta}(\tilde{X}), \tag{6.5}$$

and substitution into (6.2) gives

$$\tilde{\phi}^{\mathrm{IV}} = \frac{\mathrm{d}}{\mathrm{d}\tilde{X}}\left(\frac{\Theta'}{\Psi'}\tilde{\phi}\right), \quad \tilde{\theta} = \frac{\Theta'}{\Psi'}\tilde{\phi}. \tag{6.6}$$

The conditions

$$\tilde{\phi} = \tilde{\phi}' = 0 \quad \text{on } \tilde{X} = \pm\tfrac{1}{2}, \tag{6.7}$$

are sufficient to ensure the correct behaviours of both the velocity and temperature fields at the walls without the need for local thermal boundary layers at leading order. At the centre, $\tilde{X} = 0$, a singularity arises if $\tilde{\phi}$ is finite, due to the vanishing of the base-flow velocity Ψ', and a critical layer forms. In $\tilde{X} < 0$ the solution for $\tilde{\phi}$ can be written as

$$\tilde{\phi} = \mu_1 f_1(\tilde{X}) + \mu_2 f_2(\tilde{X}), \tag{6.8}$$

where μ_1 and μ_2 are complex constants and f_1 and f_2 are uniquely defined by

$$f_1''' = \frac{\Theta'}{\Psi'} f_1; \quad f_1 = f_1' = 0, \quad f_1'' = 1 \quad (\tilde{X} = -\tfrac{1}{2}), \tag{6.9}$$

$$f_2''' = \frac{\Theta'}{\Psi'} f_2 + 1; \quad f_2 = f_2' = f_2'' = 0 \quad (\tilde{X} = -\tfrac{1}{2}). \tag{6.10}$$

Since the base profiles Θ' and Ψ are even, the appropriate solution in $\tilde{X} > 0$ is

$$\tilde{\phi} = \nu_1 f_1(-\tilde{X}) + \nu_2 f_2(-\tilde{X}), \tag{6.11}$$

where ν_1 and ν_2 are complex constants. As $\tilde{X} \to 0-$, f_1 and f_2 have general forms

$$f_{1,2} \sim \tilde{a}_{1,2} + \tilde{b}_{1,2}\tilde{X} + \tilde{X}^2\left\{\tfrac{1}{2}\tilde{a}_{1,2}\frac{\Theta'(0)}{\Psi''(0)}\ln|\tilde{X}| + \tilde{c}_{1,2}\right\} + \tilde{d}_{1,2}\tilde{X}^3, \tag{6.12}$$

where, from (6.9), (6.10),

$$\tilde{d}_1 = \tfrac{1}{6}\tilde{b}_1\frac{\Theta'(0)}{\Psi''(0)}, \quad \tilde{d}_2 = \frac{1}{6}\left\{\tilde{b}_2\frac{\Theta'(0)}{\Psi''(0)} + 1\right\}. \tag{6.13}$$

Consideration of the flow across the critical layer, where $\tilde{X} = O(\alpha^{-\frac{1}{3}})$, leads to four bridging conditions, two of which are

$$\left.\begin{aligned}(\mu_1 + \nu_1)\tilde{b}_1 + (\mu_2 + \nu_2)\tilde{b}_2 = 0,\\ (\mu_1 + \nu_1)\tilde{d}_1 + (\mu_2 + \nu_2)\tilde{d}_2 = 0.\end{aligned}\right\} \tag{6.14}$$

The solution of interest is the one for which

$$\det\begin{pmatrix}\tilde{b}_1 & \tilde{b}_2\\ \tilde{d}_1 & \tilde{d}_2\end{pmatrix} = \tfrac{1}{6}\tilde{b}_1 = 0; \tag{6.15}$$

other possibilities correspond to regular solutions for $\tilde{\phi}$ that vanish at $\tilde{X} = 0$ and do not generally correspond to real values of α. Thus γ_c is determined by the requirement that there is a solution of (6.9) for which $f_1'(0) = 0$. The properties of Θ' and Ψ' confirm that the lowest value of γ_c occurs in the range $\gamma_a < \gamma_c < \gamma_b$, where $\gamma_a = 4.73$ is the point at which the horizontal base temperature gradient first becomes negative (i.e. $\Theta'(0) = 0$), and $\gamma_b = 7.85$ is the point at which regions of reversal of the vertical base flow first occur (i.e. $\Psi''(0) = 0$). A finite-difference computation of its value from (6.9) gave $\gamma_c = 6.30$, and the function f_1 is shown in figure 14.

The form of the neutral curve at large values of γ can also be determined analytically. The base flow and horizontal temperature variation occur entirely in boundary layers with thickness of order γ^{-1} close to the vertical walls. Near the cold wall

$$\Psi' \sim \tfrac{1}{4}\gamma^{-2}\mathrm{e}^{-\overline{X}}\sin\overline{X}, \quad \Theta \sim -\tfrac{1}{2}\mathrm{e}^{-\overline{X}}\cos\overline{X}, \tag{6.16}$$

where $\overline{X} = \gamma\tilde{x}$, and the perturbation functions ϕ and θ have local scalings

$$\phi \sim \gamma^{-3}\overline{\phi}(\overline{X}), \quad \theta \sim \overline{\theta}(\overline{X}), \tag{6.17}$$

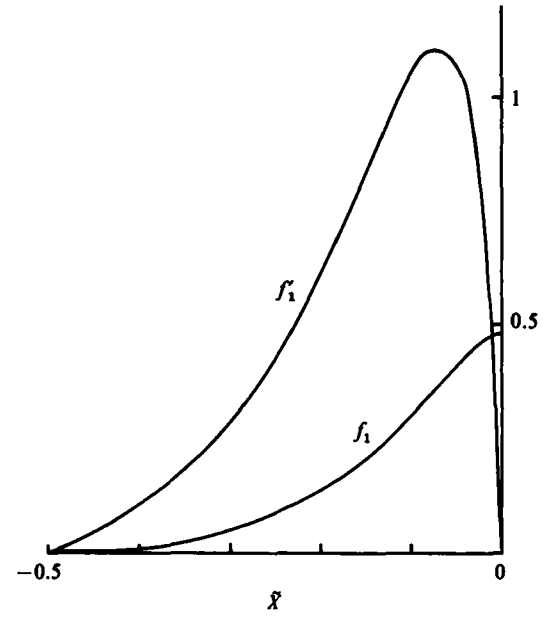

FIGURE 14. The outer function f_1 at the critical point γ_c.

with $$\alpha \sim \gamma^4 \bar{\alpha}. \tag{6.18}$$

The full stability equations (6.2) hold within the boundary-layer regions but the hot-wall layer can be ignored by invoking the symmetry conditions (6.4) which, together with (6.2), imply that in the core

$$\theta \sim \epsilon e^{ik}, \quad \phi \sim i\gamma^{-3}\lambda\epsilon e^{ik}, \tag{6.19}$$

where λ, ϵ and k are real constants. In the cold-wall layer the final problem is a limiting form of that discussed by Daniels (1985*b*) and with the outer constraint $\bar{\phi} \to i\lambda\bar{\theta}$ as $\bar{X} \to \infty$ given by (6.19), can be solved to give

$$\lambda = -0.65, \quad \bar{\alpha} = 152.3. \tag{6.20}$$

The disturbance corresponds to a vertically stratified, horizontal flow across the core which is entrained and detrained by the boundary-layer flow near each wall, forming large rolls which span the region between the vertical walls. Smaller regions of closed circulation centre on the maximum overall stream-function locations which occur within each boundary layer.

7. Discussion

The present asymptotic theory of high-Prandtl-number convection in a vertical slot suggests that a boundary-layer approximation is useful for values of the convective parameter $l = (A/h)^{\frac{1}{4}}$ less than a critical value of about 11. Solutions obtained by spectral decomposition show the development from the conductive regime, and at the centre of the slot predict a vertical-temperature-gradient maximum near $l = 6.5$ and a stream-function maximum near $l = 11$. The latter behaviour heralds the onset of an unstable region where even the reduced system appears subject to an instability in the form of transverse rolls. Numerical evidence

σ	h	$A_c \times 10^{-5}$	$(A_c/h)^{\frac{1}{4}}$	Author	Description
10^3	19	3.0	11.2	Elder (1965)	experimental
900	20	3.7	11.7	Vest & Arpaci (1969)	experimental
480	15	1.8	10.4	Seki *et al.* (1978)	experimental
10^4	4	0.42	10.1	Simpkins & Dudderar (1981)	experimental
10^3	10	2.4+	12.4+	De Vahl Davis & Mallinson (1975)	numerical
480	15	3.0	11.9	Bontoux & Roux (1982)	numerical
10^3	15	4.0−	12.8−	Lee & Korpela (1983)	numerical

TABLE 3. The onset of secondary motion for large-Prandtl-number fluids.

of this is supported by a stability analysis based on an approximation to the base flow near mid-cavity level which, taking $\beta = \frac{1}{2}$, predicts destabilization at

$$l_c = 2^{\frac{3}{4}}\gamma_c = 10.6. \tag{7.1}$$

The critical value $\gamma_c = 6.30$ obtained in §6 is virtually coincident with the attainment of the first maximum of the (approximate) stream function $\bar{\psi}(\frac{1}{2}l)$, which, from (5.12) and assuming β to be constant, is at $\gamma = 2\pi$ (further maxima and minima occur at integer multiples of 2π). At the critical point the stability calculations (and the numerical evidence – figure 10*a*) indicates the importance of wavelengths much less than the height of the slot and the need, in a complete analysis, to retain the vertical diffusion terms in the governing equations for $l \geqslant l_c$. Taking $\beta = \frac{1}{2}$ the minimum value of α given by the neutral curve of the present long-wave stability theory corresponds to about three vertically stacked anticlockwise rolls at large values of l (figure 13). The numerical scheme generally produced five, but while the discretization of the spectrum by the end conditions at $z = 0, 1$ might be expected to provide an additional constraint, realistic comparisons are not really possible. The stability theory is linear and also dependent on an approximation to the base flow that becomes less relevant at large values of l where the real flow is strongly influenced by the endwalls.

The present theory supports the view that for high-Prandtl-number fluids secondary motions arise from conditions prevailing near mid-cavity level where the horizontal flow is weakest, consistent with Elder's (1965) comment that the end-zones remain regions of strong damping. Although the stability analysis needs to be extended to account for both short-wavelength disturbances and the spatial variation of the base flow, it is of interest to compare the criterion (7.1) with experimental results for high-Prandtl-number convection. Elder (1965) concluded from his experiments that the threshold point for a vertical slot of aspect ratio h may be defined by a critical Rayleigh number

$$A = 3 \times 10^5 \pm 30\,\%, \tag{7.2}$$

whereas the present results suggest that a more appropriate measure is

$$l_c = (A/h)^{\frac{1}{4}} \approx 11. \tag{7.3}$$

A comparison with various experimental and numerical results for a range of values of A and h supports this view (see table 3) and the need for the large error margin in (7.2) is not surprising.

It is stressed that an alternative approach is needed to obtain accurate numerical solutions for $l > l_c$, and to determine whether the multiple-cell solutions (figure 10) are simply transient states triggered by the destabilization of the mid-cavity flow; a 'roll-swallowing' sequence (Bontoux & Roux 1982) could conceivably lead to a final

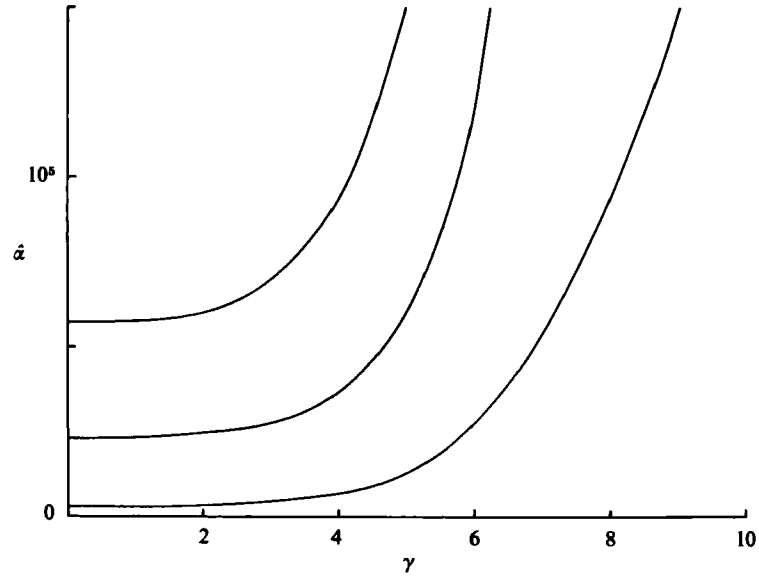

FIGURE 15. The first three real eigenvalues $\hat{\alpha} = \pm i\alpha$ of the system (6.2), (6.3).

configuration in which regions of recirculation are confined to mid-cavity level, as in numerical calculations by Rubel & Landis (1969) and in keeping with the ultimate boundary-layer structure proposed by Gill (1966) and Blythe *et al.* (1983). It seems more likely, however, in view of the stability analysis, that the vertical boundary-layer system does admit multiple solutions for $l > l_c$ and that only one of these approaches the aforementioned boundary-layer solution as $l \to \infty$. It may be added that a converged boundary-layer solution containing three cells has been obtained numerically using the present spectral approach with $x_\infty = 12$ and $N = 10$, but its relevance must remain in doubt at this level of truncation, and certainly boundary-layer solutions based on Oseen and integral methods (Gill 1966; Blythe & Simpkins 1977) show no signs of steady multiple-cell states, although both methods involve approximations that may exclude such solutions.

A final possibility is that multiple-cell states arise smoothly as l increases through l_c, with no 'simple' base state for $l > l_c$ until the boundary-layer structure evolves as $l \to \infty$. Such a smooth evolution would be expected if the real solutions $\pm\alpha$ of (6.2), (6.3) had evolved from roots with non-zero imaginary part for $\gamma < \gamma_c$, but this is not the case. The system (6.2), (6.3) has a family of roots

$$\alpha = \pm i\hat{\alpha} \quad (\hat{\alpha} \text{ real}), \tag{7.4}$$

for all values of γ (figure 15). They stem from the real family of decaying eigensolutions which characterize the flow in the conductive regime near each endwall, and the corresponding eigenvalues $\hat{\alpha} = 2.58 \times 10^3$, 2.31×10^4, 5.76×10^4,... (Daniels 1985*a*) are the limits of those shown in figure 15 as $\gamma \to 0$. The real roots $\pm\alpha$ arise instead from the passage to zero, as $\gamma \to \gamma_c -$, of a pair of complex roots of the complete stability problem equivalent to (6.2), (6.3) in which vertical diffusion is included; they therefore only arise in the vertical boundary-layer model for $\gamma > \gamma_c$ and are then additional to the complete set (7.4) that already, in principle, provides the adjustment to the end boundary conditions. Their appearance at γ_c therefore

seems most likely to correspond to a bifurcation and subsequent non-uniqueness of the steady solution.

The author is grateful for useful discussions with Professor P. A. Blythe.

REFERENCES

BATCHELOR, G. K. 1954 *Q. Appl. Maths* **12**, 209.

BERGHOLZ, R. F. 1978 *J. Fluid Mech.* **84**, 743.

BIRIKH, R. V., GERSHUNI, G. Z., ZHUKOVITSKII, E. M. & RUDAKOV, R. N. 1969 *Prikl. Math. Mekh.* **33**, 958.

BLYTHE, P. A., DANIELS, P. G. & SIMPKINS, P. G. 1983 *Proc. R. Soc. Lond.* A **387**, 367.

BLYTHE, P. A. & SIMPKINS, P. G. 1977 *Physico-Chemical Hydrodynamics* (ed. D. B. Spalding), vol. 2, p. 511. Adv. Pub. Inc.

BONTOUX, P. & ROUX, B. 1982 In *Lecture Series 9, 'Natural Convection: Theory and Experiment'*. Von Karman Institute.

CATTON, I., AYYOSWAMY, P. S. & CLEVER, R. M. 1974 *Intl J. Heat Mass Transfer* **17**, 173.

DANIELS, P. G. 1985*a* *Intl J. Heat Mass Transfer* **28**, 2071.

DANIELS, P. G. 1985*b* *Proc. R. Soc. Lond.* A **401**, 145.

DANIELS, P. G. 1986 *Q. J. Mech. Appl. Maths* (to appear).

DANIELS, P. G. & SIMPKINS, P. G. 1982 A numerical solution of the vertical boundary layer equations in a horizontally heated cavity using a spectral method. *Bell Labs. Tech. Memo.* (unpublished).

DE VAHL DAVIS, G. & MALLINSON, G. D. 1975 *J. Fluid Mech.* **72**, 87.

ECKERT, E. R. G. & CARLSON, W. O. 1961 *Intl J. Heat Mass Transfer* **2**, 106.

ELDER, J. W. 1965 *J. Fluid Mech.* **23**, 77.

ELDER, J. W. 1966 *J. Fluid Mech.* **24**, 823.

GERSHUNI, G. Z. 1953 *Zh. Tekh. Fiz.* **23**, 1838.

GILL, A. E. 1966 *J. Fluid Mech.* **26**, 515.

GILL, A. E. & DAVEY, A. 1969 *J. Fluid Mech.* **35**, 775.

GILL, A. E. & KIRKHAM, C. C. 1970 *J. Fluid Mech.* **42**, 125.

GOLDSTEIN, S. 1938 *Modern Developments in Fluid Dynamics*, vol. 2. Oxford University Press.

HART, J. E. 1971 *J. Fluid Mech.* **47**, 547.

KORPELA, S. A., GOZUM, D. & BAXI, C. B. 1973 *Intl J. Heat Mass Transfer* **16**, 1683.

KUIKEN, H. K. 1968 *J. Engng Maths* **2**, 355.

LEE, Y. & KORPELA, S. A. 1983 *J. Fluid Mech.* **126**, 91.

MIZUSHIMA, J. & GOTOH, K. 1976 *J. Fluid Mech.* **73**, 65.

MORDCHELLES-REGNIER, C. & KAPLAN, C. 1963 *Proc. Heat Transfer Fluid Mech. Inst.*, p. 94.

NUSSELT, W. 1909 *V.D.I. Forsch. Arb.* **63**, 78.

RUBEL, A. & LANDIS, F. 1969 *Phys. Fluids Suppl.* II, **12**, II–208.

RUDAKOV, R. N. 1967 *Prikl. Math. Mekh.* **31**, 376.

SEKI, N., FUKUSAKO, S. & INABA, H. J. 1978 *J. Fluid Mech.* **84**, 695.

SIMPKINS, P. G. & DUDDERAR, T. D. 1981 *J. Fluid Mech.* **110**, 433.

TOLSTOV, G. P. 1962 *Fourier Series*. Prentice Hall.

VEST, C. M. & ARPACI, V. S. 1969 *J. Fluid Mech.* **36**, 1.